

Cosmic CARNage II: the evolution of the galaxy stellar mass function in observations and galaxy formation models

Rachel Asquith,^{1*} Frazer R. Pearce,¹ Omar Almaini,¹ Alexander Knebe,^{2,3}
 Violeta Gonzalez-Perez,^{4,5} Andrew Benson,⁶ Jeremy Blaizot,^{7,8,9} Jorge Carretero,^{10,11}
 Francisco J. Castander,¹⁰ Andrea Cattaneo,¹² Sofía A. Cora,^{13,14} Darren J. Croton,¹⁵
 Julien E. Devriendt,¹⁶ Fabio Fontanot,¹⁷ Ignacio D. Gargiulo,^{13,14} Will Hartley,¹⁸
 Bruno Henriques,¹⁹ Jaehyun Lee,²⁰ Gary A. Mamon,²¹ Julian Onions,¹
 Nelson D. Padilla,^{22,23} Chris Power,²⁴ Chaichalit Srisawat,²⁵ Adam R. H. Stevens,^{15,24}
 Peter A. Thomas,²⁵ Cristian A. Vega-Martínez,¹³ Sukyoung K. Yi²⁶

¹*School of Physics & Astronomy, University of Nottingham, Nottingham NG7 2RD, UK*

²*Departamento de Física Teórica, Módulo 15, Facultad de Ciencias, Universidad Autónoma de Madrid, 28049 Madrid, Spain*

³*Centro de Investigación Avanzada en Física Fundamental (CIAFF), Facultad de Ciencias, Universidad Autónoma de Madrid, 28049 Madrid, Spain*

⁴*Institute for Computational Cosmology, Department of Physics, University of Durham, South Road, Durham, DH1 3LE, UK*

⁵*Institute of Cosmology & Gravitation, University of Portsmouth, Dennis Sciama Building, Portsmouth, PO1 3FX, UK*

⁶*Carnegie Observatories, 813 Santa Barbara Street, Pasadena, CA 91101, USA*

⁷*Université de Lyon, Lyon, F-69003, France*

⁸*Université Lyon 1, Observatoire de Lyon, 9 avenue Charles Andrè, Saint-Genis Laval, F-69230, France*

⁹*CNRS, UMR 5574, Centre de Recherche Astrophysique de Lyon ; Ecole Normale Supérieure de Lyon, Lyon, F-69007, France*

¹⁰*Institut de Ciències de l'Espai, IEEC-CSIC, Campus UAB, 08193 Bellaterra, Barcelona, Spain*

¹¹*Port d'Informació Científica (PIC) Edifici D, Universitat Autònoma de Barcelona (UAB), E-08193 Bellaterra (Barcelona), Spain.*

¹²*GEPI, Observatoire de Paris, CNRS, 61, Avenue de l'Observatoire 75014, Paris France*

¹³*Instituto de Astrofísica de La Plata (CCT La Plata, CONICET, UNLP), Paseo del Bosque s/n, B1900FWA, La Plata, Argentina.*

¹⁴*Facultad de Ciencias Astronómicas y Geofísicas, Universidad Nacional de La Plata, Paseo del Bosque s/n, B1900FWA, La Plata, Argentina*

¹⁵*Centre for Astrophysics and Supercomputing, Swinburne University of Technology, Hawthorn, Victoria 3122, Australia*

¹⁶*Astrophysics, University of Oxford, Denys Wilkinson Building, Keble Road, Oxford, OX1 3RH, UK*

¹⁷*INAF - Astronomical Observatory of Trieste, via Tiepolo 11, I-34143 Trieste, Italy*

¹⁸*Department of Physics and Astronomy, University College London, Gower Street, London WC1E 6BT*

¹⁹*Max-Planck-Institut für Astrophysik, Karl-Schwarzschild-Str. 1, 85741 Garching b. München, Germany*

²⁰*Korea Institute for Advanced Study, 85 Hoegiro Dongdaemun-gu, Seoul 02455 Korea*

²¹*Institut d'Astrophysique de Paris (UMR 7095: CNRS & UPMC), 98 bis Bd Arago, F-75014 Paris, France*

²²*Instituto de Astrofísica, Universidad Católica de Chile, Santiago, Chile*

²³*Centro de Astro-Ingeniería, Universidad Católica de Chile, Santiago, Chile*

²⁴*International Centre for Radio Astronomy Research, University of Western Australia, 35 Stirling Highway, Crawley, Western Australia 6009, Australia*

²⁵*Department of Physics & Astronomy, University of Sussex, Brighton, BN1 9QH, UK*

²⁶*Department of Astronomy and Yonsei University Observatory, Yonsei University, 03722 Seoul, Republic of Korea*

Accepted 2018 July 09. Received 2018 July 09; in original form 2017 December 19

arXiv:1807.03796v2 [astro-ph.GA] 27 Jul 2018

ABSTRACT

We present a comparison of the observed evolving galaxy stellar mass functions with the predictions of eight semi-analytic models and one halo occupation distribution model. While most models are able to fit the data at low redshift, some of them struggle to simultaneously fit observations at high redshift. We separate the galaxies into ‘passive’ and ‘star-forming’ classes and find that several of the models produce too many low-mass star-forming galaxies at high redshift compared to observations, in some cases by nearly a factor of 10 in the redshift range $2.5 < z < 3.0$. We also find important differences in the implied mass of the dark matter haloes the galaxies inhabit, by comparing with halo masses inferred from observations. Galaxies at high redshift in the models are in lower mass haloes than suggested by observations, and the star formation efficiency in low-mass haloes is higher than observed. We conclude that many of the models require a physical prescription that acts to dissociate the growth of low-mass galaxies from the growth of their dark matter haloes at high redshift.

Key words: methods:numerical – galaxies:haloes – galaxies: evolution – cosmology:theory – dark matter

1 INTRODUCTION

Locally, low-mass galaxies tend to be disk-like, blue and star-forming, whereas high-mass galaxies are more likely to be spheroidal, red and passive (e.g. Kennicutt 1998; Strateva et al. 2001; Kauffmann et al. 2003; Baldry et al. 2004). At high redshift ($z > 1$) we also observe this bimodality in the galaxy population (Kovač et al. 2014; Cirasuolo et al. 2007), but do not definitively know the mechanisms by which these galaxies evolve into the populations we observe locally. Various mechanisms have been suggested to move galaxies from the ‘blue cloud’ to the ‘red sequence’ and shut off their star formation in a process known as ‘quenching’. Potential quenching mechanisms include environmental effects and feedback from active galactic nuclei (AGN) at high masses (for a review see Benson 2010), but these processes are still not fully understood.

One way to study this problem is to directly observe galaxies forming and evolving in the distant Universe. At high redshift ($z > 1$), deep near-infrared observations are vital to select galaxies by rest-frame optical light. Selecting high-redshift galaxies using optical imaging will introduce strong biases against dusty galaxies or those with evolved (i.e. passive) stellar populations (e.g. Cowie et al. 1996). It is only recently that deep near-infrared surveys have been conducted with the required depth and area to produce large galaxy samples at high redshift, sufficient to allow accurate determinations of the galaxy stellar mass function while minimising the influence of cosmic variance. In particular, the UKIDSS Ultra Deep Survey (UDS) (Lawrence et al. 2007, Almaini et al. in prep.) and UltraVISTA (McCracken et al. 2012) are now deep enough to detect typical (i.e. M^*) galaxies to $z \sim 3$, over large volumes of the distant Universe ($\sim 100 \times 100$ projected comoving Mpc at $z = 3$). Using these surveys, we can directly test model predictions for the build-up of the galaxy populations, rather than inferring their evolution by extrapolating back in time. However, each galaxy is only being seen at one point in its life and we cannot infer the full evolutionary history.

In order to get a cohesive picture of what happens to galaxies throughout their lives, one approach is to link a population of galaxies at high redshift to a population at low redshift that could be their descendants. This can be done by selecting galaxies at a constant comoving number density when ranked by mass or luminosity (Mundy et al. 2015). This method was partly motivated by the need to overcome ‘progenitor bias’, where new young star-forming galaxies enter the sample at low redshift that are not present at high redshift (Shankar et al. 2015). Not accounting for this bias correctly can lead to a poor selection of the set of galaxies being connected as progenitor and descendent and therefore incorrect conclusions being drawn about their evolution.

A powerful method to trace galaxies through redshift is to use semi-analytic models (SAMs) (for a review see Benson 2010; Somerville & Davé 2015), a type of galaxy formation model in which simple analytic prescriptions (in connection with merger trees from either cosmological simulations or extended Press-Schechter formalisms) are used to model the physical processes occurring during galaxy formation and evolution. These models are able to evolve the same population of galaxies through redshift and connect them without the limitations of observational methods. These models are also computationally inexpensive, so can be used to simulate large volumes and produce large catalogues of galaxies with which to compare observational data. By comparing the models to key observables, e.g. the evolution of the stellar mass function (SMF), we can learn about the physics of galaxy formation. If models are not able to reproduce observational results it may mean that they are missing key physics which is important in galaxy formation and evolution. Model galaxies can also be separated into ‘star-forming’ and ‘passive’ types, to test for the quenching processes which transform galaxies from star-forming to passive.

While it has been shown that SAMs are able to reproduce the SMF at $z = 0$, they struggle to simultaneously match observations at both low and high redshift (e.g. Fontanot et al. 2009; Weinmann et al. 2012; Guo et al. 2011; Knebe et al. 2015). This has only become clearer in recent years as observational surveys have been able to probe

* E-mail: rachel.asquith@nottingham.ac.uk

down to lower masses as well as probing to higher redshifts. Observational evidence appears to point towards a seemingly ‘anti-hierarchical’ formation scenario where high-mass galaxies form earlier with their abundance changing little from $z \sim 1$ to the present day, whereas there is a rapid evolution in the number of low-mass galaxies at late times (e.g. Fontana et al. 2004, 2006; Faber et al. 2007; Pozzetti et al. 2007; Marchesini et al. 2009, 2010; Pozzetti et al. 2010; Ilbert et al. 2010, 2013; Muzzin et al. 2013). This is sometimes referred to as ‘mass assembly downsizing’ (Cowie et al. 1996; Cimatti et al. 2006; Lee & Yi 2013).

After much work understanding both AGN feedback and the mass assembly of high-mass galaxies (e.g. Benson et al. 2003; Di Matteo et al. 2005; Bower et al. 2006; Croton et al. 2006), models are now able to reproduce the high-mass end of the galaxy stellar mass function over a range of redshifts. However, models still typically overproduce the number of low-mass galaxies at high redshift. The main reason for this discrepancy appears to be that galaxies in the models follow the growth of their dark matter haloes too closely (Weinmann et al. 2012; Somerville & Davé 2015; Guo et al. 2016). Halo mass growth is the main driver of gas accretion rate in galaxies, which then in turn drives the star formation rate. The star formation history then traces the dark matter mass accretion history, which, in the favoured Λ CDM structure formation scenario, is approximately self-similar for haloes of different masses. However, in the real Universe it appears that there is not such a tight correlation (White et al. 2015; Guo et al. 2016).

This excess of low-mass galaxies at high redshift was investigated by Fontanot et al. (2009), who found that in three different SAMs, galaxies in the mass range $9 < \log(M_*/M_\odot) < 11$ form too early and have little ongoing star formation at late times. They concluded that the physical processes operating on these mass scales, such as supernova feedback, needed a re-think. Weinmann et al. (2012) later used two SAMs and two cosmological hydrodynamical simulations and examined the evolution of the observed number density of galaxies. They found that although the models fit well at $z = 0$, the low-mass galaxies were formed at early times. They conclude that as the current form of feedback is mainly dependent on host halo mass and time, it is unlikely to be able to separate the growth of galaxies from the growth of their dark matter haloes.

Monte Carlo Markov Chain (MCMC) methods were used by Henriques et al. (2013) in an attempt to fit the stellar mass function at all redshifts, but they could not find a single set of parameters that allowed this. They then changed the reincorporation timescale for ejected gas to be inversely proportional to halo mass and independent of redshift and found that they were able to fit observed numbers of low-mass galaxies from $0 < z < 3$. However, the passive fraction of low-mass galaxies was still too high. Their model was later updated further in Henriques et al. (2015) where they also reduce ram-pressure stripping in low-mass haloes, make radio-mode AGN feedback more efficient at low redshift, and reduce the gas surface density threshold for star formation. They then find that their model reproduces the observed abundance and passive fraction of low-mass galaxies, both at high and low redshift.

Another attempt to solve this problem was by White et al. (2015), who tried three different physically motivated

methods to decouple the accretion rate in galaxies from their star formation rate. They found that changing the gas accretion to be less efficient in low-mass haloes at early times and increasing the dependence of stellar feedback on halo mass at high redshift were the most successful at qualitatively matching the evolution of the number density of low-mass galaxies. However, they allow these functions to scale with halo mass and redshift in an arbitrary way which may not be physically motivated. Hirschmann et al. (2016) also investigated this problem with their model and found that they improved their agreement with observations by either reducing the gas ejection rate with cosmic time or varying the reincorporation timescale with halo mass, classed as ‘ejective’ and ‘preventative’ feedback schemes respectively. Although their results improve from their fiducial model, they still find too many low-mass, red, old galaxies between $0.5 < z < 2.0$.

However, the effect of adjusting certain physical prescriptions can be vastly different between models. White et al. (2015) investigated what effect replicating the changes in Henriques et al. (2013) had on their own model, but found that it did not make much difference to the observed number density of low-mass galaxies. They conclude that this is due to the sensitivity of the results to how the gas reservoirs are tracked and treated in the different codes. Croton et al. (2016) also had similar problems with this approach and found that it did not solve the problems with fitting the stellar mass function. This presents difficulties to the modelling community, as it means that different models may require different changes to get them to match the observed evolution.

It is also possible to try and match the galaxy stellar mass function at all redshifts without changing the physics involved in the model. For example, Rodrigues et al. (2017) used GALFORM to identify a small region of parameter space where the model matched the observational data out to $z = 1.5$, without needing to adapt any of the physics involved. They found that the parameters controlling the feedback processes were most strongly constrained, suggesting that these processes are important when fitting the evolution of the galaxy stellar mass function.

Halo occupation distribution (HOD) models, rather than modelling the physical processes that we think go into galaxy formation, use statistical methods to match galaxies to their corresponding dark matter haloes (e.g. Berlind & Weinberg 2002; Zheng et al. 2005). As these models are applied independently at each redshift, the evolution of each galaxy is not tracked, although they can be connected to their progenitors and descendants via dark matter merger trees. HOD models by design are able to reproduce the SMF at each redshift and are therefore able to reproduce the population of galaxies at any given time. This type of model is a very useful tool for learning about the relationship between galaxies and their host dark matter haloes and how this changes as a function of redshift. For example, Berlind et al. (2003) found that low-mass haloes are mainly populated by young galaxies and high-mass haloes by older galaxies.

Galaxy formation models such as HODs and SAMs must be calibrated using observational datasets. Varying the calibration dataset, *even for the same model* may produce significantly different catalogues. Essentially, the calibration datasets introduce tension, and it may not be possible for a single model to fit all the required observational datasets

simultaneously. This could be because the model lacks some of the required physics or that the underlying observational datasets are incomplete or are physically incompatible with each other.

In the Cosmic CARNage mock galaxy comparison project (Knebe et al. 2018, hereafter referred to as Paper I) we sought to address some of these issues by requiring the participants to calibrate their models to the same set of observational data. These data included the galaxy stellar mass function at $z = 0$ and $z = 2$, the star formation rate function at $z = 0.15$, the black-hole bulge-mass relation at $z = 0$, and the cold gas mass fraction at $z = 0$. Participants were free to weight these five calibrations as they saw fit, and were asked to generate their “best-fit” model that took all of them into account, i.e. calibration set ‘c02’ in Paper I.

We will build on previous work by investigating the evolution of the SMF for the eight SAMs and one HOD model that were used in Paper I. These models are all calibrated to the same observational data and are all run on the same background dark matter only simulation, which means that we can discount the differences due to the underlying cosmological framework when considering the differences between the models. Our aim is then to see if the current physical prescriptions used in any of the galaxy formation models can produce a realistic population of galaxies at both low and high redshift. We will investigate the evolution of the SMF in the redshift range $0.5 < z < 3.0$ for all nine galaxy formation models and determine if models still struggle to simultaneously match observations both at low and high redshift.

The rest of this paper is structured as follows: in Section 2 we will briefly explain the underlying dark matter simulation and the parameters used. In Section 3 we will present the results for the evolution of the SMF and the passive fraction. We will then show how the specific star formation rate of star-forming galaxies in the models evolves. We will also examine the average halo mass as a function of stellar mass and the stellar mass - halo mass relation for all the models. In Section 4 we will present our discussion and in Section 5 we will present our conclusions.

2 SIMULATION DATA

The eight SAMs we will be using are DLB07 (De Lucia & Blaizot 2007), GALFORM (Gonzalez-Perez et al. 2014), GALICS-2.0 (Cattaneo et al. 2017, although the exact version used for this comparison is the one described in the appendix of Knebe et al. (2015)), LGALAXIES (Henriques et al. 2013), MORGANA (Monaco et al. 2007), SAG (Cora et al. 2018), SAGE (Croton et al. 2016) and γ SAM (Lee & Yi 2013). The single HOD model is MICE (Carretero et al. 2015). A brief description of the physical prescriptions used in each model is given in the Appendix of Knebe et al. (2015). Any changes to any of the models since then are included in Appendix A.

The models have all been run on the same underlying dark matter simulation which may be different to the one used in the above reference papers. This can lead to changes in the predictions of each model, as can varying the initial mass function, yield, stellar population synthesis model and calibration data set used.

A description of how the models were calibrated to the same observational data is given in Paper I. We also note that the stellar masses from the models have been convolved with a $0.08(1+z)$ dex scatter to account for the observational errors when measuring stellar mass. This value comes from Conroy et al. (2009), who estimate an error of ~ 0.2 dex at $z = 2$ when fixing the stellar population synthesis model.

The underlying cosmological dark-matter-only simulation was run using the GADGET-3 N -body code (Springel 2005) with parameters given by the Planck cosmology (Planck Collaboration et al. 2014, $\Omega_m = 0.307$, $\Omega_\Lambda = 0.693$, $\Omega_b = 0.048$, $\sigma_8 = 0.829$, $h = 0.677$, $n_s = 0.96$). We use 512^3 particles of mass $1.24 \times 10^9 h^{-1} M_\odot$ in a box of comoving width $125h^{-1} \text{Mpc}$. The halo catalogues were extracted from 125 snapshots and identified using ROCKSTAR (Behroozi et al. 2013a). The halo merger trees were then generated using the CONSISTENT TREES code (Behroozi et al. 2013b).

3 RESULTS

3.1 Evolution of the Galaxy Stellar Mass Function

We start by examining the evolution of the stellar mass function in Figure 1, shown for the whole sample in the top row. The coloured lines are the stellar mass functions for each of the models, computed for each redshift bin using single snapshots at $z = 0.8, 2.0$ and 3.0 for each redshift bin respectively. We note that the precise choice of snapshot does not affect our conclusions. The observations from Davidzon et al. (2017) are based on the UltraVISTA near-infrared survey of the COSMOS field and are shown as a black line and dark shaded region. When finding the best-fit Schechter parameters to their stellar mass functions, they take into account the errors in measuring stellar mass, known as Eddington bias. As they have applied this correction, when plotting the stellar mass function we do not apply the $0.08(1+z)$ dex scatter to the stellar mass values. In Appendix B we have included a version of Figure 1 where the model stellar masses do have this scatter applied, to show the differences to the SMF.

We also note that we compare to different observational data than the combined dataset used to calibrate the models. The data from Davidzon et al. (2017) is more recent than the calibration dataset and also allows us to split our sample into passive and star-forming galaxies. When comparing Davidzon et al. (2017) to the stellar mass function calibration data at $z = 0$ and $z = 2$, the two largely agree, although the former has smaller error bars. This is encouraging as it shows good agreement between different observations.

Inspecting the top panels, what is clear is that the observational number counts are evolving, with the high-mass end largely in place by $z = 3$, while the low-mass end rises at late times. Whilst the models match the observations well at low redshift, the strong evolution at the low-mass end is not seen for most of the galaxy formation models. The exceptions to this are MICE, LGALAXIES and SAG, which all show an increasing number density of low-mass galaxies towards low redshift. As MICE is an HOD model it has been designed to match the evolution of the SMF. LGALAXIES and SAG likely do a better job of matching the SMF at high redshift due to the physics involved in the treatment of gas. Both

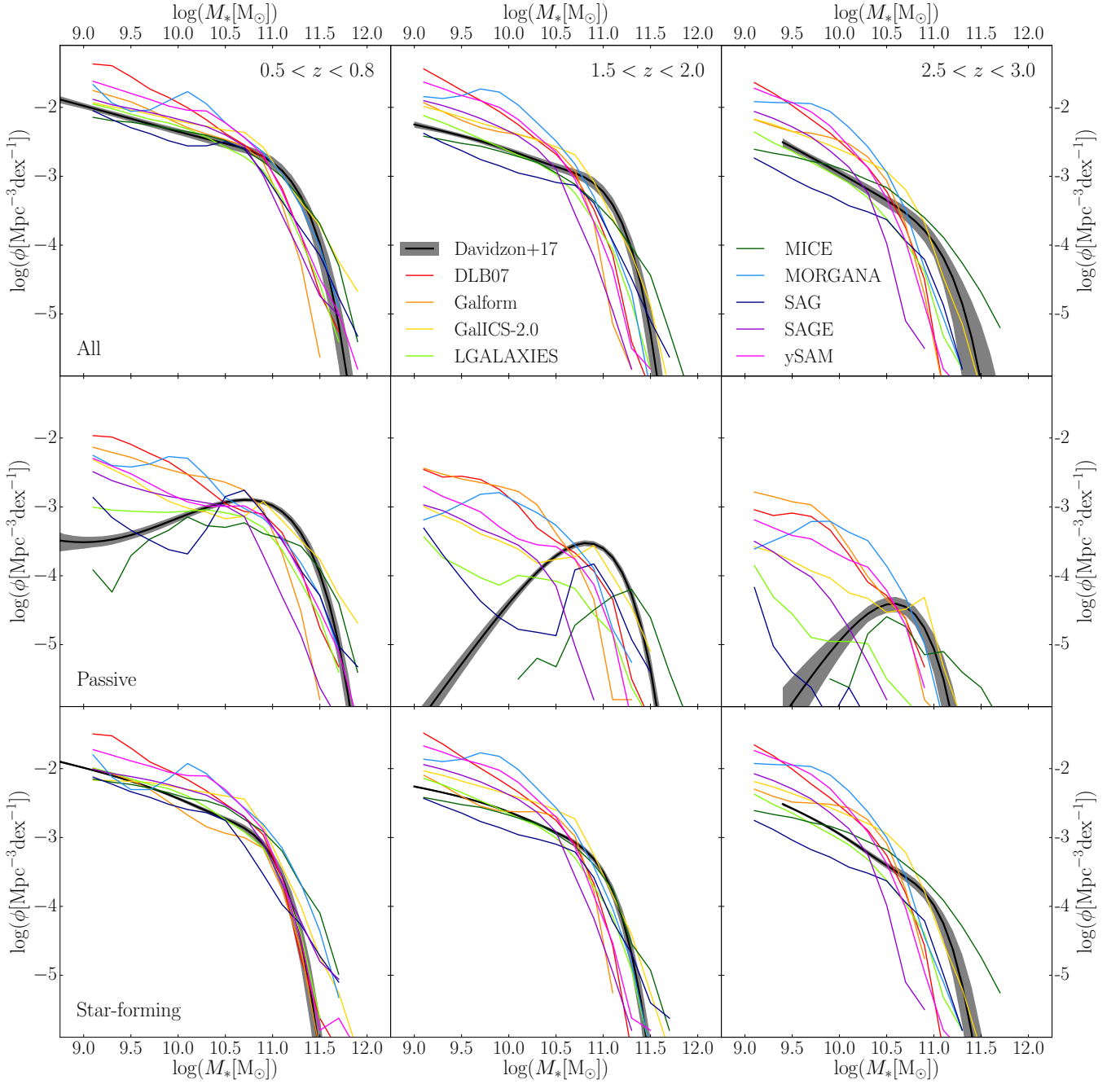


Figure 1. The evolution of the stellar mass function for all the models over the range $0.5 < z < 3.0$. The stellar mass function for the whole, passive and star-forming samples are shown in the top, middle and bottom panels, respectively, as coloured lines. The black line is the observational best-fit mass functions from [Davidzon et al. \(2017\)](#), with the dark grey shaded region showing the 1σ errors. For the models, each redshift bin contains one snapshot, at redshifts $z = 0.8, 2.0$ and 3.0 respectively. We can see that the models match well at low redshift (by construction), but deviate further from the observations at high redshift. The number density of the lowest mass objects is nearly constant in the models but changes by more than 0.5 dex in the observations. Most of the low-mass galaxies that are not present in the observations at high redshift seem to be star-forming.

follow the prescription suggested in [Henriques et al. \(2013\)](#) of scaling the reincorporation timescale of ejected gas with the inverse of the halo mass. This means the process of gas being reincorporated back into the halo takes longer for low-mass haloes, shifting the growth of galaxies in these haloes from early to late times. SAG also scales the reheated and

ejected mass with redshift to make supernova feedback more efficient at high redshift.

At the high-mass end, the models underestimate the number density compared to observations, with MICE and GALICS-2.0 as the exceptions. One alternative reason for this tension at the high-mass end may be due to [Davidzon et al. \(2017\)](#) underestimating their uncertainties when

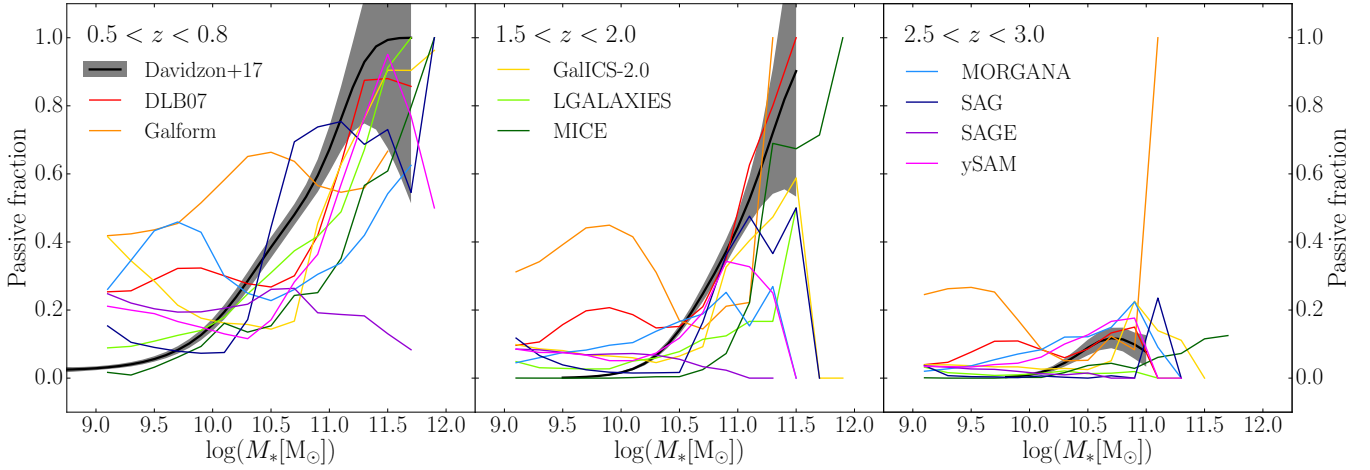


Figure 2. The evolution of the passive fraction over the range $0.5 < z < 3.0$. The coloured lines, black solid lines and grey shaded regions are the same as in Figure 1, as are the snapshots used in each redshift bin for the models. For a few models the passive fraction is too high at low masses, particularly at low redshift. The models match well at high masses at low redshift, but generally underpredict the passive fraction for high-mass galaxies at high redshift.

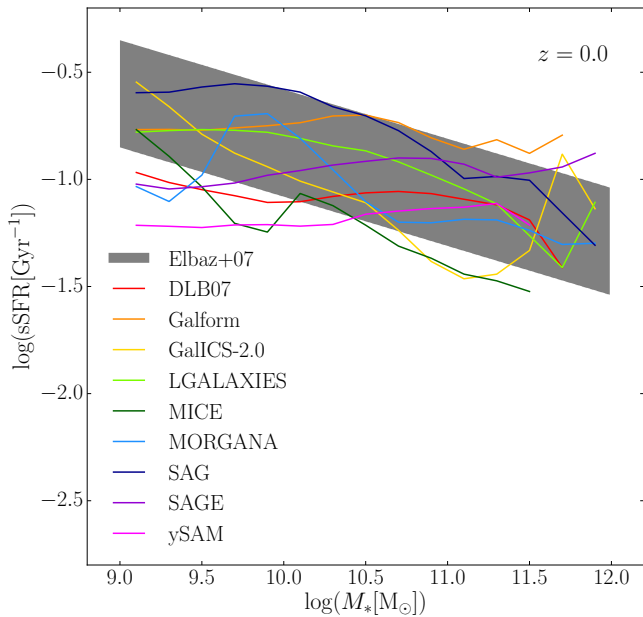


Figure 3. The relationship between mass and sSFR at $z = 0.0$ for star-forming galaxies in the nine models. The model data is taken from one snapshot at $z = 0.0$. The grey shaded region is taken from Elbaz et al. (2007) and shows the observational best-fit to this relation. The sSFR of star-forming galaxies in the models matches observations well but there is less of a trend with mass in some models.

accounting for Eddington bias, as it is very difficult to accurately measure all of the sources of error. Due to the steep slope of the SMF at high masses this would have a greater impact at the high-mass end of the SMF. The impact of Eddington bias on the SMF are discussed further in Appendix B.

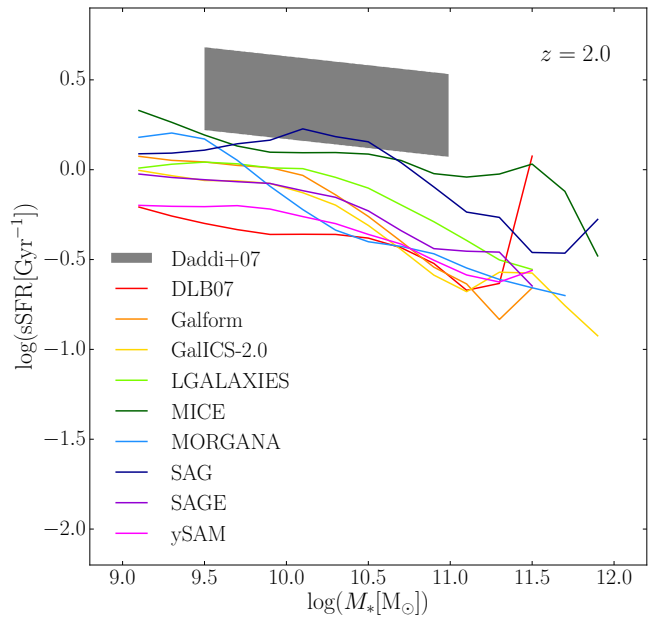


Figure 4. As for Figure 3, but for $z = 2.0$ and observations from Daddi et al. (2007). The model data is taken from one snapshot at $z = 2.0$. Here all of the models lie almost completely below the observational best-fit range.

3.2 Star-forming and Passive Galaxy Stellar Mass Functions

We explore the mass growth further in the bottom two rows of Figure 1, splitting the population into passive (middle row) and star-forming (bottom row) galaxies. We separate passive and star-forming galaxies using a redshift-dependent specific star formation rate (sSFR) cut of $\text{sSFR}(z) = 1/(3t_{\text{H}}(z))$ where $t_{\text{H}}(z)$ is the Hubble time at that redshift. We test the robustness of this cut by examining the change in our results when using slightly different cuts of $\text{sSFR}(z) =$

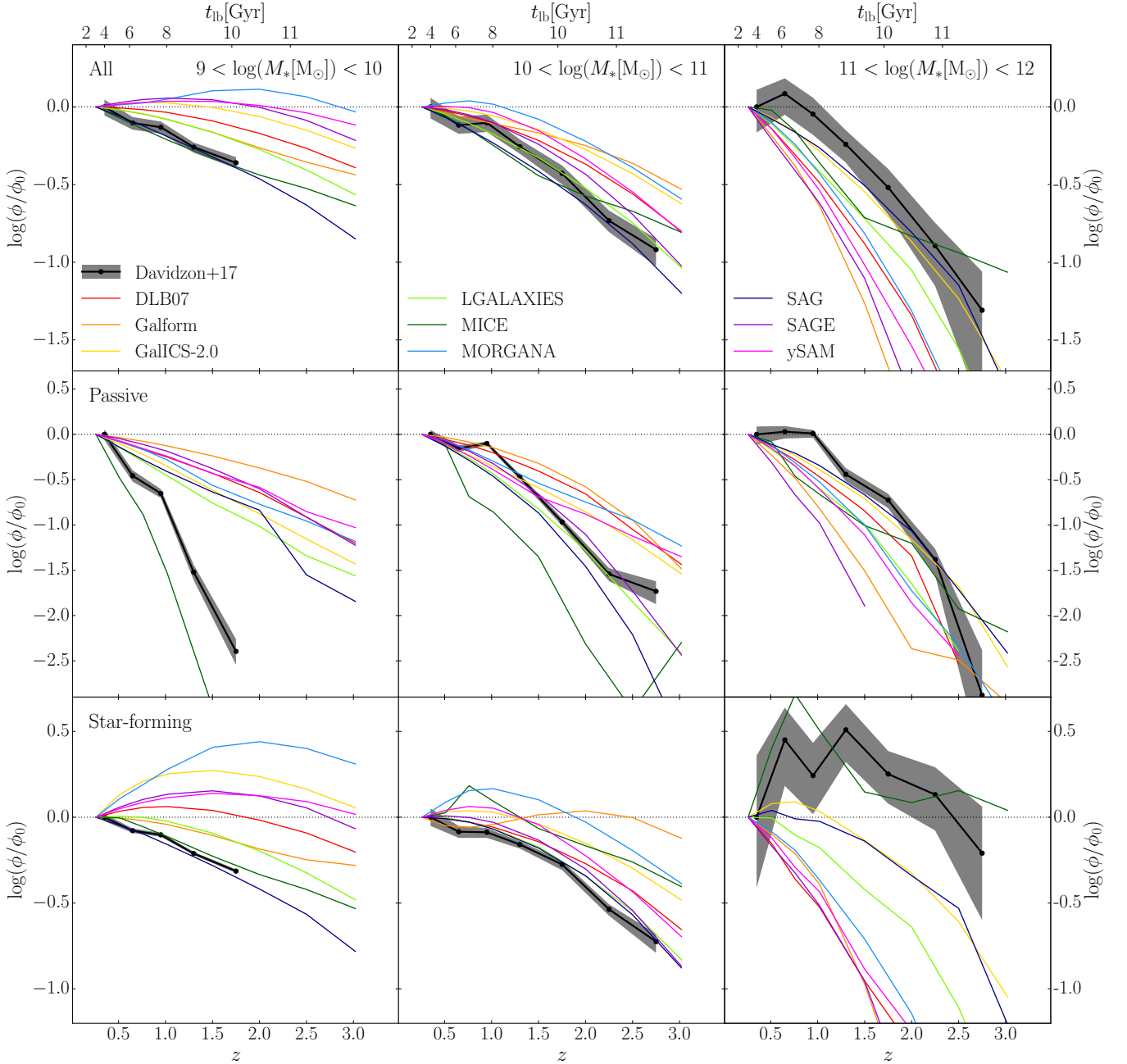


Figure 5. The evolution of the number density ϕ , in bins of stellar mass. This is normalised by the number density at $0.2 < z < 0.5$, which we call ϕ_0 . We show three mass bins as indicated (left to right panels) for all galaxies (top panels), passive galaxies (middle panels) and star-forming galaxies (bottom panels). The dark grey shaded regions and black lines with circular points show data from [Davidzon et al. \(2017\)](#). The coloured points and lines are for the nine models. In the lowest mass bin, most of the models assemble the galaxies before the observations. The models match the observations well at intermediate masses, but the observational number density increases before many of the models at high mass.

$1/(2t_{\text{H}}(z))$ and $\text{sSFR}(z) = 1/(4t_{\text{H}}(z))$. We find that the shape of the stellar mass function changes very little and makes no difference to any of the conclusions that we draw. In the observations the passive and star-forming galaxies are separated using the (NUV - r) vs (r - J) colour-colour diagram as described in [Ilbert et al. \(2013\)](#), which is best suited to differentiate fully quiescent galaxies from those with residual star formation. In practice, the exact location of the split makes little difference to the low-mass end of the star-forming SMF

and the high-mass end of the passive SMF, as these galaxies will have very blue and red colours respectively.

Splitting the galaxy population in this way reveals that the main source of the difference between the observations and the models comes from the star-forming population: low-mass star-forming galaxies appear to be far too common at high redshift in the models and the star-forming SMF evolves little from $z = 3$ to $z = 0.5$. The exceptions to this are MICE and LGALAXIES, which appear consistent with

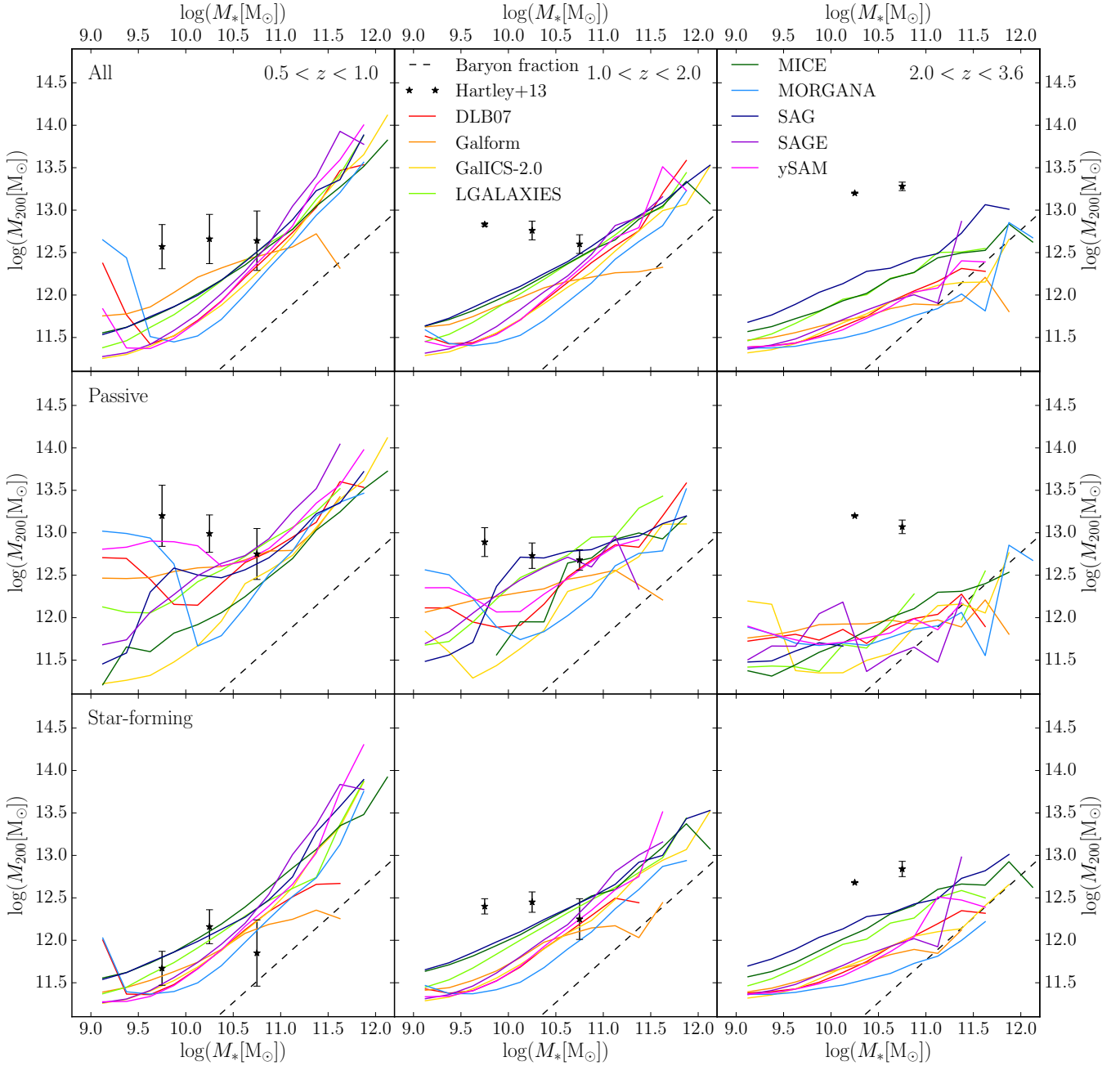


Figure 6. The average halo mass in the models compared to measurements from observations between $z = 0.5$ and $z = 3.6$. Observational measurements of the average halo mass from [Hartley et al. \(2013\)](#) are derived from clustering and are shown as stars. The values for each model are shown as coloured lines. For the models, the mass of the main host halo was used rather than the subhalo, to better compare with observational halo mass measurements from clustering. The top panels cover the full galaxy sample, the middle panels are for passive galaxies and the bottom panels are for star-forming galaxies. The black dashed line shows the universal baryon fraction. For the models, we use snapshots at $z = 1.0, 2.0$ and 3.5 for each redshift bin respectively. For the passive sample, the halo masses from observations are approximately constant, but decrease by up to a factor of 10 in the models with increasing redshift. For the star-forming sample, the observations show halo mass increasing with increasing redshift, whereas in the models there is no real trend with redshift.

the observations at low masses up to $z = 3$. For the passive galaxies, the number density at low masses does evolve with redshift in the models, as seen in the observations. However, most of the SAMs show rising number density towards lower masses, in contrast with the observations which appear to show a turnover or flattening of the passive SMF towards lower masses. In order to solve these problems, models need

to find a physically motivated way to reduce the star formation rates of low-mass galaxies at high redshift. The same galaxies at later times would then have lower stellar masses and star formation rates. This would then act to redistribute the passive SMF in the models to better match the observations.

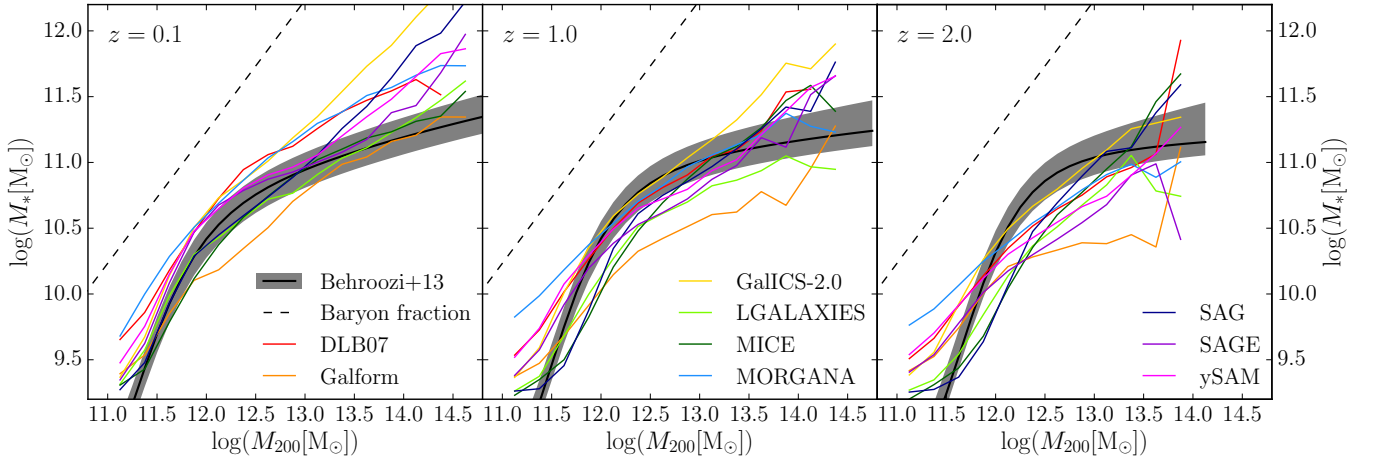


Figure 7. Comparison of the average stellar mass for each halo mass bin in the models to the abundance matching model of Behroozi et al. (2013c), considering only central galaxies. The results from the models are shown as coloured lines and the stellar mass - halo mass relation from Behroozi et al. (2013c) is shown as a dark grey shaded region and black line. The black dashed line shows the universal baryon fraction. The panels are for each redshift, increasing from left to right, using snapshots at $z = 0.0, 1.0$ and 2.0 respectively. Looking at the data from Behroozi et al. (2013c), we can see that the average stellar mass stays fairly constant with redshift, but increases in the models towards low redshift, particularly at high masses.

3.3 Evolution of the Passive Fraction

Another way of looking at this result is to examine the passive fraction, which is shown in Figure 2. Again, the shaded regions indicate the observations taken from the same source as used for Figure 1. The passive fraction indicates the ratio of passive to star-forming galaxies. At low masses, some of the models, such as DLB07, GALFORM and MORGANA, tend to overestimate the passive fraction compared to observations. This has been seen previously and appears to be linked to how environmental processes are taken into account in the models (Lagos et al. 2014; Gonzalez-Perez et al. 2018). At low redshift the number of star-forming galaxies matches observations well, so this difference is due to the lack of a turnover or flattening of the passive SMF. At higher redshifts, the overproduction of low-mass star-forming galaxies would act to decrease the passive fractions. However, this is still too high in some models, again due to the rising number density towards low masses in the passive SMF.

At low redshift, the models tend to match the observations well at high masses, but one model, SAGE, underpredicts the passive fraction. This is mainly due to an underprediction for the number of high-mass passive galaxies. As shown by Stevens & Brown (2017), detailing the structural evolution of galaxy discs with the DARK SAGE variant of the model (Stevens et al. 2016) leads to more sensible passive fractions. In the redshift range $1.5 < z < 2.0$ the models tend to underpredict the fraction of high-mass galaxies, mainly due to the lack of high-mass passive galaxies above $z \sim 1$. The model which best matches the observed passive fraction for high-mass galaxies is DLB07, which slightly underpredicts the number density of both high-mass passive and star-forming galaxies in this redshift range.

3.4 Relationship between Mass and Specific Star Formation Rate

In order to better compare star formation in the observations and the models, we also look at the specific star formation rates of the subset of star-forming galaxies. Figure 3 shows the average sSFR as a function of mass at $z = 0.0$ for each of the models as a solid coloured line. The grey shaded region is taken from Elbaz et al. (2007), who used SDSS data to find a fit to the correlation between SFR and mass at $z = 0$. Their sample is made up of 19590 galaxies with redshifts $z = 0.04-0.1$ and is complete to $M_B \leq -20$. Brinchmann et al. (2004) used H_α emission to derive the SFR of these galaxies and the stellar masses were derived by Kauffmann et al. (2003), who fit using a library of star formation histories to find the most likely stellar mass.

Most of the models match the observations well here, with LGALAXIES and SAG lying in the observational region at all masses. Some models appear to evolve less with mass than the observations suggest, with some showing almost no trend, whereas the sSFR implied by the observations decreases by over 0.5 dex between $10^9 M_\odot$ and $10^{12} M_\odot$. This means that some of the models, such as GALFORM, match at low masses but not high masses, and others such as DLB07 and ySAM match at high masses but not low masses. This was also discussed in Guo et al. (2016), who used data from two SAMs, GALFORM and LGALAXIES, and one hydrodynamical simulation, EAGLE. They found that the median sSFR remained almost constant with mass, in contrast with observations.

The relationship between sSFR and stellar mass at $z = 2.0$ is then shown in Figure 4. Here the observations are taken from Daddi et al. (2007), who use galaxies in the GOODS-S field to find the correlation between SFR and mass at $z = 2$. They are complete to $K < 22$ and use only $24\mu\text{m}$ selected galaxies in order to exclude passive galaxies. The SFRs were estimated using the UV and the stellar masses were derived by Fontana et al. (2004) using SED fitting.

This comparison highlights large differences between the observations and models at this redshift, with the models almost completely outside the observational range. The sSFR of star-forming galaxies in the models is on average around 0.5 dex lower than measured in the observations. The models therefore predict a slower evolution of the sSFR with redshift than observations. This has been previously seen by [Mitchell et al. \(2014\)](#), who find that when they scale the reincorporation time of gas with redshift they are able to better match the evolution of the stellar mass function, but still underestimate the sSFR of high-mass galaxies at $z \sim 2$. [Hirschmann et al. \(2016\)](#) also found that their ejective models predicted lower than observed sSFRs at high redshift, even when they could reproduce the growth of the stellar mass function.

Reducing the star formation rates of galaxies above $z \sim 2$, as suggested in Section 3.2, may help to solve this problem. If galaxies have a lower star formation rate at higher redshift, their resulting mass at lower redshift will be lower. A galaxy with the same star-formation rate at $z = 2$ will then have a higher sSFR as it will have a lower stellar mass.

3.5 Growth of the Galaxy Stellar Mass Function

In Figure 5 we examine the growth of the stellar mass function as a function of mass and redshift. This is found by taking the value of the number density ϕ at fixed stellar mass for a certain redshift bin and normalising it by the value of ϕ in the lowest redshift bin $0.2 < z < 0.5$, which we call ϕ_0 . This allows for easier comparison between the models and observations and will highlight when the number density of different populations increases. The dark grey region and black line with circular points shows data from [Davidzon et al. \(2017\)](#). The coloured lines then show the number density evolution for the nine models. The black dotted line shows where the number density is equal to the number density in the lowest redshift bin.

Looking at the passive galaxies, we can see that the models struggle to match the observed growth of the mass function at low masses, as the number density of low-mass galaxies increases in the models at higher redshift than the observations. The only exception is MICE, which has very few galaxies with mass below $10^{10}M_{\odot}$ above $z \sim 1$. At intermediate masses the models match the observations well, but at high masses the growth of the mass function occurs in observations before many of the models.

For the star-forming galaxies, at low masses there is a similar problem with several of the models; the mass function grows too much at high redshift. Just under half of the models have more low-mass star-forming objects in the highest redshift bin than the lowest redshift one. However, several of the models are more in line with the growth of the observed mass function, namely SAG and MICE. At intermediate masses, the number density of star-forming galaxies increases at higher redshift in the models than in the observations. The model that is most discrepant, MORGANA, has more intermediate mass star-forming galaxies between $1.0 < z < 1.5$ than in the lowest redshift bin. For high-mass galaxies, the number density evolves little since high redshift in the observations. MICE reproduces this trend well but in other models the number density increases at lower redshift. This may be in part due to the fact that there are

low numbers of the highest mass galaxies which will naturally introduce more scatter in the proportional change in number density.

We can also see interesting differences between models when comparing the stellar mass function to the growth of the stellar mass function. Looking at the lower panel of Figure 1, we can see that DLB07 overpredicts the number of low-mass star-forming galaxies at both low and high redshift. SAGE agrees well with observations at low redshift but overproduces low-mass star-forming galaxies at high redshift. However, looking at the lower left panel of Figure 5, we can see that DLB07 matches observations of the growth of the mass function better than SAGE. These models therefore have slightly different problems; DLB07 has too many low-mass galaxies at all redshifts, but the number density increases at the correct rate. Conversely, SAGE has the correct number at low redshift, but the number density increases too early.

3.6 Average Halo Mass

In this section we study the average halo mass the galaxies reside within, shown in Figure 6. For the models we use single snapshots at $z = 1.0, 2.0$ and 3.5 for each redshift bin respectively. The dashed black line indicates the universal baryon fraction, i.e. where all the baryonic material within the halo has been converted into stars. Each of the coloured lines indicates the average halo mass values for a different model, while the black points with errorbars are average halo mass values taken from [Hartley et al. \(2013\)](#), who use the UDS DR8 data to estimate the halo masses from measurements of galaxy clustering (e.g. [Mo & White 2002](#), and references therein).

For the models, here we use the mass of the main host halo for each galaxy rather than the mass of its subhalo. Host haloes do not reside within another halo, whereas subhaloes are contained within a host halo. Although using the host halo is not necessarily the usual choice when analysing simulation data, it allows us to compare to observational measurements of halo mass from galaxy clustering, which effectively measure the mass of the main host haloes ([Mo & White 2002](#)). For this reason we also include both centrals and satellites, in order to best mimic the observational measurements. Assuming galaxy clustering measurements can correctly recover the host halo mass, we can then directly compare the observations and models.

Splitting the sample into passive and star-forming galaxies in Figure 6 we see that there are marked differences between the observations and the models. For passive galaxies, the average halo mass in observations stays constant over redshift in the observations, but rises towards low redshift in the models. For the star-forming population, while the observations indicate a general downsizing trend in halo mass of about an order of magnitude between high and low redshift, all the models show virtually no change. It is clear that the models start significantly below the observations at $2.0 < z < 3.5$ and only agree with the observations by $0.5 < z < 1.0$. Both passive and star-forming low-mass galaxies are therefore in lower mass haloes on average in the models than in the observations at high redshift.

One thing that can affect the average halo mass values in the models is the halo mass definition used, as this can

lead to differences of up to 20 percent (Jiang et al. 2014). Although this may account for some of the scatter between the models, the differences between the observations and models cannot be explained by this alone. Another factor that could affect the observational measurements of halo mass from clustering is ‘halo assembly bias’, which refers to the fact that halo clustering can depend on other properties besides halo mass. For example, Gao et al. (2005) found that at fixed halo mass, haloes that assembled earlier are more clustered than those that assembled later. Therefore, galaxies in older haloes will be more strongly clustered than they should be for their halo mass, which means that their halo masses will be measured as higher than they actually are. This could alleviate some of the discrepancy between the observations and models. For example, if the passive galaxies observed at low redshift are associated to older haloes, then their halo masses could have been overestimated.

3.7 Stellar Mass - Halo Mass Relation

In Figure 7 we display measurements of the average stellar mass of central galaxies in bins of halo mass, comparing the models with the abundance matching model of Behroozi et al. (2013c). The dashed black line indicates the universal baryon fraction and the dark grey region and black solid line show the fit to the stellar mass - halo mass (SMHM) relation from Behroozi et al. (2013c). The coloured lines show the average stellar mass values for each different model.

At low redshift, the results from the models and the SMHM relation agree well at low and intermediate halo masses. However, above halo masses of $\sim 10^{13.5}M_{\odot}$ the average stellar mass of centrals in the models is higher than suggested by the SMHM relation. This means that at low redshift, star formation in high-mass haloes is more efficient in the models. The exceptions to this are LGALAXIES and MICE, which agree with the SMHM relation at nearly all halo masses. For most of the models, the slope of the relation at high halo masses does flatten, but not to the extent seen from the SMHM relation.

As we move to higher redshift the SMHM relation changes little. The peak of the relation moves to slightly higher halo masses and the average stellar mass for low-mass haloes decreases by ~ 0.4 dex at $10^{11.5}M_{\odot}$. In the models the average stellar mass for low-mass haloes decreases slightly with increasing redshift, but is above the SMHM relation by $z = 1.0$ for most models. This discrepancy can be partially explained by the cut in stellar mass applied at $M_* = 10^9 M_{\odot} h^{-1}$, which may have skewed the distribution towards higher stellar masses. This might be enough to explain the difference for models such as LGALAXIES or GALFORM, but the discrepancy is too large for MORGANA, DLB07 and γ SAM. In these models, the average stellar mass for low-mass haloes at high redshift is too high. This means that star formation in these objects is very efficient, leading to an increase in the number of low-mass galaxies at $z \sim 2$. This is likely due to the way that the physics involved in the gas cycle is implemented in these models.

For intermediate- and high-mass haloes, the average stellar mass generally decreases with increasing redshift in the models and the slope of the relation decreases. This suggests that star formation was less efficient in the models at high redshift. At $z = 0.1$ the models overpredict the stellar

mass in high-mass haloes, but slightly underpredict it by $z = 2.0$. For intermediate-mass haloes, the average stellar mass is too low in the models at $z = 2.0$ by up to 0.5 dex, as is the case for GALFORM at $10^{12.5}M_{\odot}$. The model that changes the least with redshift is MICE; as this is an HOD model it naturally matches the SMHM relation better than the SAMs.

4 DISCUSSION

Comparing several galaxy formation models allows us to distinguish areas that are challenging for the current generation of models and therefore provide direction for the future development of the field as a whole. The main issue highlighted in this paper is the fact that most of the models produce too many low-mass, star-forming galaxies at early times. Observationally these appear either to not exist or to be missed by the surveys. This is a difficult area observationally with the answer to this question only becoming evident when the stellar mass functions are reliably pushed to lower masses. At present they are tantalisingly close to indicating a clear turnover in the space density of passive galaxies at low-mass, which would significantly challenge many of the models featured here.

In the absence of a new population of low-mass, star-forming galaxies being observed at $z \sim 2$, many of the models would need improvements in order to reproduce observations. They would need to produce far fewer low-mass star-forming galaxies at essentially all but the latest times. Shifting star formation from high-mass haloes at high redshift to low-mass haloes at low redshift would also produce better agreement with observations of galaxy clustering. Reducing the number of low-mass star-forming objects would also have to be achieved without reducing the number of high-mass objects significantly.

Some of the models, such as LGALAXIES and SAG, do fit the low-mass end of both the star-forming and passive stellar mass function at high redshift. This is likely due to their implementation of the physics involved in the treatment of gas, in particular the reincorporation timescales. MICE also matches observations at high redshift, but as this is a HOD model it matches by construction. However, there are still some observables that even these models struggle to match, such as the relation between stellar mass and specific star formation rate and the average halo mass that galaxies occupy. Whilst this could be due to problems with the observational measurements of these quantities, this could point towards areas where the models still need to improve.

5 CONCLUSIONS

In this paper we have contrasted nine different galaxy formation models and compared them to the latest high-redshift observations. In doing so we have highlighted the areas in which the models find particular difficulty in matching the observations. We can see from this project that some of the models still have trouble simultaneously matching the stellar mass function at both low and high redshift. The galaxies look roughly correct at $z = 0$, but for many models there are too many low-mass galaxies at $z \sim 2$, as has also been seen

previously (e.g. Fontana et al. 2006; Fontanot et al. 2009; Weinmann et al. 2012; Henriques et al. 2012; Guo et al. 2016).

To explore this further, we split galaxies into passive and star-forming populations. We find that there are too many star-forming galaxies with stellar masses below $10^{11}M_{\odot}$ in many of the models at $z \sim 2$.

In summary, while some of the models are remarkably successful at reproducing the evolution of the stellar mass function, there remain significant issues. In particular:

- Whilst most of the models are able to match the observed stellar mass function at low redshift, they tend to overproduce the number density of low-mass galaxies at high redshift.

- In most of the models the low-mass end of the star-forming stellar mass function is already largely in place at high redshift ($z > 1$), in contrast to observations. This is because the models appear to produce too many star-forming galaxies below the knee of the stellar-mass function at early times.

- The passive stellar mass function from the models evolves with redshift as in the observations, but does not have the same turnover or flattening in the number density at the low-mass end.

- Whilst most of the models match the passive fraction well at high masses, for some of the models the passive fraction is too high at low masses. This is despite the overproduction of low-mass star-forming galaxies.

- Most of the models are able to reproduce the relationship between sSFR and the mass of the star-forming galaxies at low redshift, but underpredict the sSFR at high redshift.

- Observational measurements of halo mass, estimated from galaxy clustering, indicate clear downsizing in the average halo mass occupied by star-forming galaxies as a function of redshift. This is not clearly indicated by any of the models; both star-forming and passive galaxies in the models occupy haloes with lower masses than those inferred from observations at $z = 2$.

- The average stellar mass is higher in low-mass haloes at high redshift in the models compared to observations, meaning that star formation in low-mass haloes is more efficient in the models than in the real Universe.

Achieving consistent results at both $z = 0$ and $z = 2$ with a population of galaxies that evolves strongly with redshift is clearly difficult. The HOD model, MICE, obtains good results but the galaxies present at $z = 2$ are not evolved directly into the $z = 0$ population. Of the SAMs, the LGALAXIES and SAG models best match the growth of the observed mass functions, but they share the same trends as the other models for the specific star formation rate and average halo mass within which the objects reside. Both of these models found that they needed to modify the treatment of the gas cycle in order to match the evolution of the low-mass end of the stellar mass function. This is very promising for the galaxy formation modelling community, which has long struggled with this issue.

While it is clear that current galaxy formation models can reproduce a variety of observational data, we have identified key areas of tension. Some models still overpredict the number of low-mass galaxies at high redshift, but even the models that can match the evolution of the galaxy stellar

mass function underpredict the specific star formation rates of galaxies at early times. Future observational surveys at high redshift will help shed light on these issues and identify further areas of improvement for the models.

ACKNOWLEDGEMENTS

We thank the anonymous referee whose comments helped to greatly improve this paper. We would also like to thank Rachel Somerville, Gabriella De Lucia and Pierluigi Monaco for kindly providing useful discussion and comments.

We thank Carnegie Observatories for their support and hospitality during the workshop ‘Cosmic CARNage’ where all the calibration issues were discussed and the roadmap laid out for the work presented here.

The authors would further like to express special thanks to the Instituto de Fisica Teorica (IFT-UAM/CSIC in Madrid) for its hospitality and support, via the Centro de Excelencia Severo Ochoa Program under Grant No. SEV-2012-0249, during the three week workshop ‘nIFTy Cosmology’ where this work developed. We further acknowledge the financial support of the 2014 University of Western Australia Research Collaboration Award for ‘Fast Approximate Synthetic Universes for the SKA’, the ARC Centre of Excellence for All Sky Astrophysics (CAASTRO) grant number CE110001020, and the ARC Discovery Project DP140100198. We also recognise support from the Universidad Autonoma de Madrid (UAM) for the workshop infrastructure.

RA is funded by the *Science and Technology Funding Council* (STFC) through a studentship. AK is supported by the *Ministerio de Economía y Competitividad* and the *Fondo Europeo de Desarrollo Regional* (MINECO/FEDER, UE) in Spain through grant AYA2015-63810-P. He further thanks Denison Witmer for california brown and blue. VGP acknowledges support from a European Research Council Starting Grant (DEGAS-259586). This work used the DiRAC Data Centric system at Durham University, operated by the Institute for Computational Cosmology on behalf of the STFC DiRAC HPC Facility (www.dirac.ac.uk). This equipment was funded by BIS National E-infrastructure capital grant ST/K00042X/1, STFC capital grant ST/H008519/1, and STFC DiRAC Operations grant ST/K003267/1 and Durham University. DiRAC is part of the National E-Infrastructure. FJC acknowledges support from the Spanish Ministerio de Economía y Competitividad project AYA2012-39620. SAC acknowledges funding from *Consejo Nacional de Investigaciones Científicas y Técnicas* (CONICET, PIP-0387), *Agencia Nacional de Promoción Científica y Tecnológica* (ANPCyT, PICT-2013-0317), and *Universidad Nacional de La Plata* (G11-124), Argentina. DJC acknowledges receipt of a QEII Fellowship from the Australian Government. FF acknowledges financial contribution from the grants PRIN MIUR 2009 ‘The Intergalactic Medium as a probe of the growth of cosmic structures’ and PRIN INAF 2010 ‘From the dawn of galaxy formation’. The work of BH was supported by Advanced Grant 246797 GALFORMOD from the European Research Council. NDP was supported by BASAL PFB-06 CATA, and Fondecyt 1150300. Part of the calculations presented here were run using the Geryon cluster at

the Center for Astro-Engineering at U. Católica, which received funding from QUIMAL 130008 and Fondecup AIC-57. CP acknowledges support of the Australian Research Council (ARC) through Future Fellowship FT130100041 and Discovery Project DP140100198. WC and CP acknowledge support of ARC DP130100117. PAT acknowledges support from the Science and Technology Facilities Council (grant number ST/L000652/1). SKY acknowledges support from the Korean National Research Foundation (NRF-2017R1A2A1A05001116). This study was performed under the umbrella of the joint collaboration between Yonsei University Observatory and the Korean Astronomy and Space Science Institute. The supercomputing time for the numerical simulations was kindly provided by KISTI (KSC-2014-G2-003).

The authors contributed to this paper in the following ways: RA analysed the data, created the plots and wrote the paper along with FRP and OA. AK & CP formed part of the core team and along with FRP organised the nIFTy workshop where this work was initiated. AB organised the follow-up workshop ‘Cosmic CARNage’ where all the discussions about the common calibration took place and out of which this paper emerged. JO supplied the simulation, halo catalogue and merger tree for the work presented here. WH supplied the halo mass measurements from the UDS that were used in this work. The remaining authors performed the SAM or HOD modelling using their codes, in particular FJC, AC, SC, DC, FF, VGP, BH, JL, ARHS, CVM, and SKY actively ran their models. All authors proof-read and commented on the paper.

This research has made use of NASA’s Astrophysics Data System (ADS) and the arXiv preprint server.

References

- Baldry I. K., Glazebrook K., Brinkmann J., Ivezić Ž., Lupton R. H., Nichol R. C., Szalay A. S., 2004, *ApJ*, 600, 681
- Behroozi P. S., Wechsler R. H., Wu H.-Y., 2013a, *ApJ*, 762, 109
- Behroozi P. S., Wechsler R. H., Wu H.-Y., Busha M. T., Klypin A. A., Primack J. R., 2013b, *ApJ*, 763, 18
- Behroozi P. S., Wechsler R. H., Conroy C., 2013c, *ApJ*, 770, 57
- Benson A. J., 2010, *Phys. Rep.*, 495, 33
- Benson A. J., Bower R. G., Frenk C. S., Lacey C. G., Baugh C. M., Cole S., 2003, *ApJ*, 599, 38
- Berlind A. A., Weinberg D. H., 2002, *ApJ*, 575, 587
- Berlind A. A., et al., 2003, *ApJ*, 593, 1
- Bower R. G., Benson A. J., Malbon R., Helly J. C., Frenk C. S., Baugh C. M., Cole S., Lacey C. G., 2006, *MNRAS*, 370, 645
- Brinchmann J., Charlot S., White S. D. M., Tremonti C., Kauffmann G., Heckman T., Brinkmann J., 2004, *MNRAS*, 351, 1151
- Carretero J., Castander F. J., Gaztañaga E., Crocce M., Fosalba P., 2015, *MNRAS*, 447, 646
- Cattaneo A., et al., 2017, *MNRAS*, 471, 1401
- Cimatti A., Daddi E., Renzini A., 2006, *A&A*, 453, L29
- Cirasuolo M., et al., 2007, *MNRAS*, 380, 585
- Conroy C., Gunn J. E., White M., 2009, *ApJ*, 699, 486
- Cora S. A., et al., 2018, *MNRAS*, 479, 2
- Cowie L. L., Songaila A., Hu E. M., Cohen J. G., 1996, *AJ*, 112, 839
- Croton D. J., et al., 2006, *MNRAS*, 365, 11
- Croton D. J., et al., 2016, *ApJS*, 222, 22
- Daddi E., et al., 2007, *ApJ*, 670, 156
- Davidzon I., et al., 2017, *A&A*, 605, A70
- De Lucia G., Blaizot J., 2007, *MNRAS*, 375, 2
- Di Matteo T., Springel V., Hernquist L., 2005, *Nature*, 433, 604
- Elbaz D., et al., 2007, *A&A*, 468, 33
- Faber S. M., et al., 2007, *ApJ*, 665, 265
- Fontana A., et al., 2004, *A&A*, 424, 23
- Fontana A., et al., 2006, *A&A*, 459, 745
- Fontanot F., De Lucia G., Monaco P., Somerville R. S., Santini P., 2009, *MNRAS*, 397, 1776
- Gan J., Kang X., van den Bosch F. C., Hou J., 2010, *MNRAS*, 408, 2201
- Gao L., Springel V., White S. D. M., 2005, *MNRAS*, 363, L66
- Gonzalez-Perez V., Lacey C. G., Baugh C. M., Lagos C. D. P., Helly J., Campbell D. J. R., Mitchell P. D., 2014, *MNRAS*, 439, 264
- Gonzalez-Perez V., et al., 2018, *MNRAS*, 474, 4024
- Gunn J. E., Gott J. R. I., 1972, *ApJ*, 176, 1
- Guo Q., et al., 2011, *MNRAS*, 413, 101
- Guo Q., et al., 2016, *MNRAS*, 461, 3457
- Hartley W. G., et al., 2013, *MNRAS*, 431, 3045
- Henriques B. M. B., White S. D. M., Lemson G., Thomas P. A., Guo Q., Marleau G.-D., Overzier R. A., 2012, *MNRAS*, 421, 2904
- Henriques B. M. B., White S. D. M., Thomas P. A., Angulo R. E., Guo Q., Lemson G., Springel V., 2013, *MNRAS*, 431, 3373
- Henriques B. M. B., White S. D. M., Thomas P. A., Angulo R., Guo Q., Lemson G., Springel V., Overzier R., 2015, *MNRAS*, 451, 2663
- Hirschmann M., De Lucia G., Fontanot F., 2016, *MNRAS*, 461, 1760
- Ilbert O., et al., 2010, *ApJ*, 709, 644
- Ilbert O., et al., 2013, *A&A*, 556, A55
- Jiang L., Helly J. C., Cole S., Frenk C. S., 2014, *MNRAS*, 440, 2115
- Kauffmann G., et al., 2003, *MNRAS*, 341, 33
- Kennicutt Jr. R. C., 1998, *ARA&A*, 36, 189
- Kimm T., Yi S. K., Khochfar S., 2011, *ApJ*, 729, 11
- Knebe A., et al., 2015, *MNRAS*, 451, 4029
- Knebe A., et al., 2018, *MNRAS*, 475, 2936
- Kovač K., et al., 2014, *MNRAS*, 438, 717
- Lagos C. D. P., Baugh C. M., Zwaan M. A., Lacey C. G., Gonzalez-Perez V., Power C., Swinbank A. M., van Kampen E., 2014, *MNRAS*, 440, 920
- Lawrence A., et al., 2007, *MNRAS*, 379, 1599
- Lee J., Yi S. K., 2013, *ApJ*, 766, 38
- Marchesini D., van Dokkum P. G., Förster Schreiber N. M., Franx M., Labbé I., Wuyts S., 2009, *ApJ*, 701, 1765
- Marchesini D., et al., 2010, *ApJ*, 725, 1277
- McCarthy I. G., Frenk C. S., Font A. S., Lacey C. G., Bower R. G., Mitchell N. L., Balogh M. L., Theuns T., 2008, *MNRAS*, 383, 593
- McCracken H. J., et al., 2012, *A&A*, 544, A156
- Mitchell P. D., Lacey C. G., Cole S., Baugh C. M., 2014, *MNRAS*, 444, 2637
- Mo H. J., White S. D. M., 2002, *MNRAS*, 336, 112
- Monaco P., Fontanot F., Taffoni G., 2007, *MNRAS*, 375, 1189
- Mundy C. J., Conselice C. J., Owersworth J. R., 2015, *MNRAS*, 450, 3696
- Muratov A. L., Kereš D., Faucher-Giguère C.-A., Hopkins P. F., Quataert E., Murray N., 2015, *MNRAS*, 454, 2691
- Muzzin A., et al., 2013, *ApJ*, 777, 18
- Planck Collaboration et al., 2014, *A&A*, 571, A16
- Pozzetti L., et al., 2007, *A&A*, 474, 443
- Pozzetti L., et al., 2010, *A&A*, 523, A13
- Rodrigues L. F. S., Vernon I., Bower R. G., 2017, *MNRAS*, 466, 2418
- Shankar F., et al., 2015, *ApJ*, 802, 73
- Somerville R. S., Davé R., 2015, *ARA&A*, 53, 51
- Springel V., 2005, *MNRAS*, 364, 1105

- Stevens A. R. H., Brown T., 2017, *MNRAS*, 471, 447
 Stevens A. R. H., Croton D. J., Mutch S. J., 2016, *MNRAS*, 461, 859
 Strateva I., et al., 2001, *AJ*, 122, 1861
 Tecce T. E., Cora S. A., Tissera P. B., Abadi M. G., Lagos C. D. P., 2010, *MNRAS*, 408, 2008
 Weinmann S. M., Pasquali A., Oppenheimer B. D., Finlator K., Mendel J. T., Crain R. A., Macciò A. V., 2012, *MNRAS*, 426, 2797
 White C. E., Somerville R. S., Ferguson H. C., 2015, *ApJ*, 799, 201
 Zheng Z., et al., 2005, *ApJ*, 633, 791

APPENDIX A: GALAXY FORMATION MODELS

A description of the physical prescriptions of each model is available in the Appendix of [Knebe et al. \(2015\)](#). Here we present a brief description of the changes to any of the models since then:

A1 SAG

The changes implemented in SAG are described in detail in [Cora et al. \(2018\)](#). We summarize them here:

Cooling Both central and satellite galaxies experience gas cooling processes. Satellite galaxies keep their hot gas haloes which are gradually removed by the action of ram pressure stripping (RPS), modelled according to [McCarthy et al. \(2008\)](#), and tidal stripping (TS). When the mass of the hot gas halo becomes smaller than 10 percent of the total baryonic mass of the galaxy, it is assumed that it no longer shields the cold gas disc from the action of RPS, which is modelled following the criterion from [Gunn & Gott \(1972\)](#); see [Tecce et al. \(2010\)](#) for more details. Values of ram pressure experienced by galaxies in haloes of different mass as a function of halo-centric distance and redshift are obtained from fitting formulae derived from the self-consistent information provided by the hydrodynamical simulations analysed by [Tecce et al. \(2010\)](#), as described in [Vega-Martínez et al. \(in prep.\)](#).

Supernova feedback and winds The mass reheated by supernova feedback involves an explicit redshift dependence and an additional modulation with virial velocity, according to a fit to results from FIRE (Feedback in Realistic Environments) hydrodynamical simulations ([Muratov et al. 2015](#)).

Gas ejection and reincorporation The energy input by massive stars eject some of the hot gas out of the halo, according to the energy conservation argument presented by [Guo et al. \(2011\)](#). The energy injected by massive stars is proportional to the mean kinetic energy of supernova ejecta per unit mass of stars formed, and includes the same explicit redshift dependence and the additional modulation with virial velocity as the reheated mass. The ejected gas mass is reincorporated back onto the corresponding (sub)halo within a timescale that depends on the inverse of the (sub)halo mass ([Henriques et al. 2013](#)).

AGN feedback AGN are produced from the growth of central BHs. When this growth takes place from cold gas accretion during gas cooling, it depends on the mass of the hot gas atmosphere, following [Henriques et al. \(2015\)](#).

Orphans The positions and velocities of orphan galaxies are obtained from the integration of the orbits of subhaloes that will not longer be identified. The orbits are integrated numerically, considering the last known position, velocity and virial mass of subhaloes as initial conditions, and taking into account mass loss by TS and dynamical friction effects, following some aspects of the works by [Gan et al. \(2010\)](#) and [Kimm et al. \(2011\)](#). A merger event occurs when the halo-centric distance becomes smaller than 10 percent of the virial radius of the host halo.

A2 SAGE

The only change in SAGE is to the radio mode AGN feedback. It is explained in detail in [Croton et al. \(2016\)](#) and summarized here:

AGN feedback The radio mode AGN feedback has been modified in SAGE since [Croton et al. \(2006\)](#). There is now a heating radius, inside which gas is prevented from cooling. This heating radius increases with subsequent heating episodes and can not decrease.

APPENDIX B: STELLAR MASS FUNCTION INCLUDING EDDINGTON BIAS

In [Figure 1](#) we have compared the stellar mass function from the models to observational data from [Davidzon et al. \(2017\)](#). We do not scatter the stellar masses in the models with the $0.08(1+z)$ dex scatter used to mimic observational uncertainties, as [Davidzon et al. \(2017\)](#) have accounted for this when finding the best-fit Schechter parameters to their stellar mass function.

Here we present an alternative version of [Figure 1](#), shown in [Figure B1](#), where we do apply the scatter to the stellar mass values in the models. We compare to observations from [Muzzin et al. \(2013\)](#), who do not take these uncertainties into account when fitting to the stellar mass function. Like [Davidzon et al. \(2017\)](#), the observations from [Muzzin et al. \(2013\)](#) are based on the UltraVISTA near-infrared survey of the COSMOS field.

Comparing [Figure B1](#) to [Figure 1](#), we can see that the main difference to the SMF is at the high-mass end and that the low-mass end is largely unaffected. Due to the redshift dependence of the scatter we apply to the stellar masses, the differences are also larger at high redshift. As an example, the value of ϕ increases by over 0.5 dex at $10^{11}M_{\odot}$ in the redshift bin $2.5 < z < 3.0$ in LGALAXIES when the scatter is applied.

In [Figure 1](#), it appears that most of the models under-predict the number of high-mass galaxies at high redshift, with only MICE and GALICS-2.0 matching observations. However, in [Figure B1](#) the models and observations agree better at high redshift for several other models, namely GALFORM and MORGANA. The data from [Muzzin et al. \(2013\)](#)

form part of the combined dataset used to calibrate the models, so it is natural that the models may match this data better.

This paper has been typeset from a $\text{T}_{\text{E}}\text{X}/\text{L}^{\text{A}}\text{T}_{\text{E}}\text{X}$ file prepared by the author.

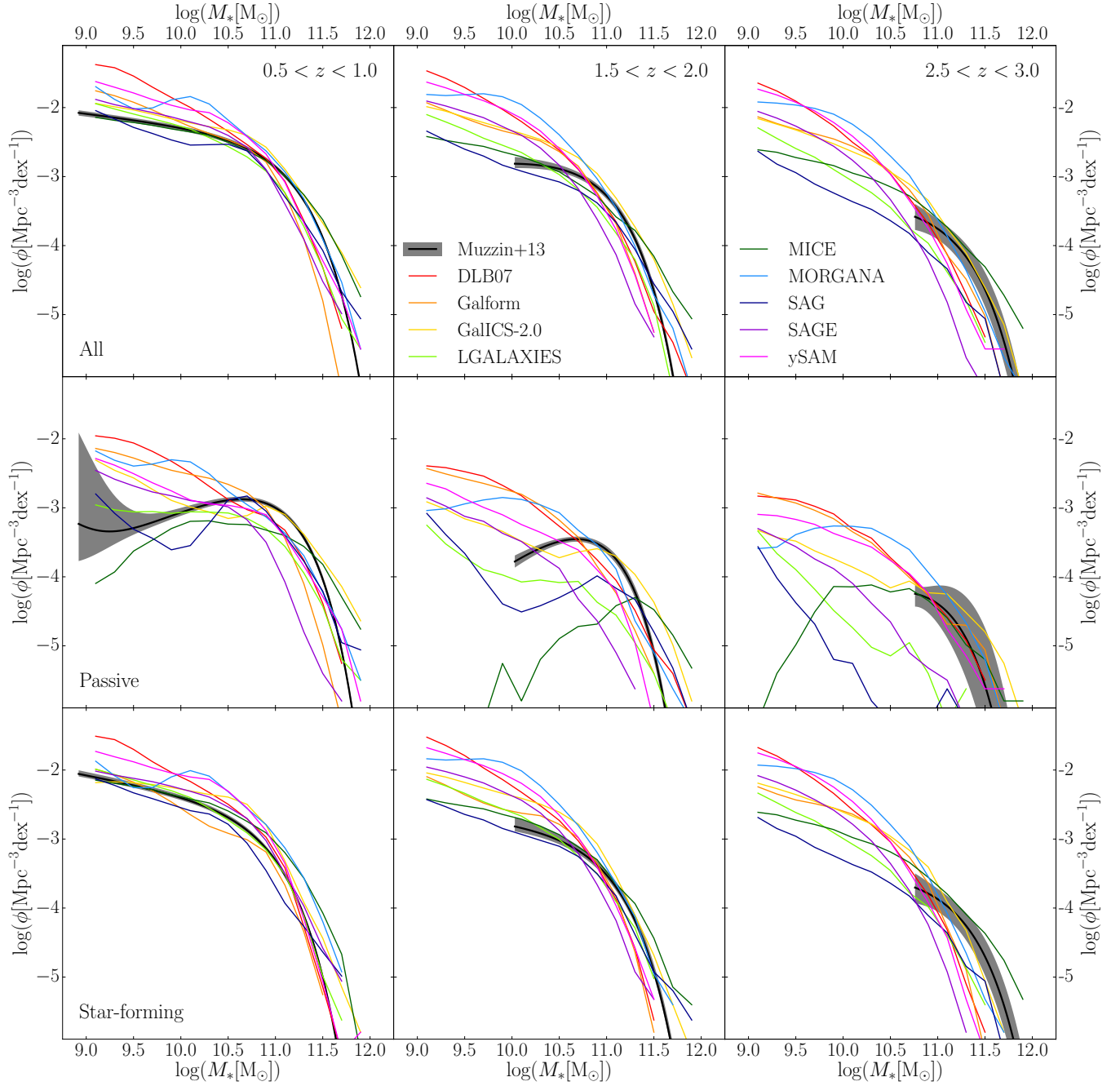


Figure B1. Alternative version of Figure 1, applying the $0.08(1+z)$ dex scatter to the stellar mass values in the models. Here we compare to observational data from [Muzzin et al. \(2013\)](#), who do not take into account Eddington bias when finding the best-fit Schechter parameters. Here the models match the observations better at high masses and high redshift.